Inorganic Chemistry
Cite This: Inorg. Chem. XXXX, XXX, XXX−XXX
Article
pubs.acs.org/IC

Efficient Visible-to-NIR Spectral Conversion for Polycrystalline Si Solar Cells and Revisiting the Energy Transfer Mechanism from Ce^{3+} to Yb^{3+} in $Lu_3Al_5O_{12}$ Host

Dan Wu,[†] Xiaoling Dong,[†] Wenge Xiao,*[,‡] Zhendong Hao,[§] and Jiahua Zhang*[,§]

[†]School of Physical Science and Technology, Inner Mongolia Key Lab of Nanoscience and Nanotechnology, Inner Mongolia University, Hohhot 010021, China

[‡]College of Optical Science and Engineering, State Key Laboratory of Modern Optical Instrumentation, Zhejiang University, Hangzhou 310027, China

[§]State Key Laboratory of Luminescence and Applications, Changchun Institute of Optics, Fine Mechanics and Physics, Chinese Academy of Sciences, 3888 Eastern South Lake Road, Changchun 130033, China

Supporting Information

ABSTRACT: The so-called Shockley−Queisser converting efficiency limit of Si solar cells is believed to be surpassed by using the spectral converter. However, searching for efficient spectral converting materials is still a challenging task. In this paper, efficient visible-to-NIR spectral conversion for polycrystalline Si solar cells has been demonstrated in Ce^{3+} and Yb^{3+} codoped $Lu_3Al_5O_{12}$. Moreover, the underlying energy transfermechanism from Ce^{3+} to Yb^{3+} is systematically re-investigated by the detailed excitation and emission spectra as well as fluorescent decay curves, and our results demonstrate that fast metal-to-metal charge transfer from Ce^{3+} to nearby Yb^{3+} is the dominant energy transfermechanism. Finally, we provide new evidence that Ce^{4+}-Yb^{2+} charge-transfer state is responsible for the relatively low quantum efficiency of NIR emission in Ce^{3+} and Yb^{3+} codoped system.

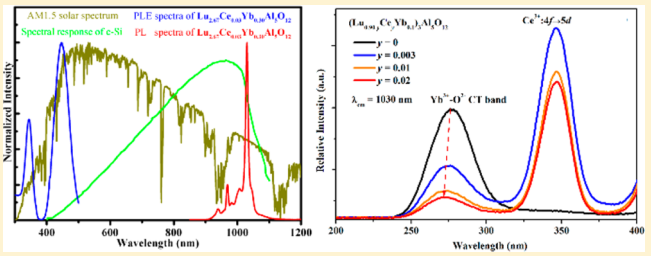

INTRODUCTION

At present, the photovoltaic market is dominated by the single-junction crystalline and polycrystalline Si solar cells. However, the theoretical maximum converting efficiency (the so-called Shockley−Queisser limit) of Si solar cells is nearly 30% because of the spectral mismatch between the solar spectrum and the spectral response of solar cells.[1,2] Therefore, many efforts have been paid to search for an efficient spectral converter in order to break such efficiency limit of Si solar cells, including downconversion from the UV and Visible photons to near-infrared (NIR) photons,[3,4] and upconversion from those longer NIR photons to NIR photons around 1100 nm.[5,6] However, all the materials for spectral conversion are still far from practical applications. Compared with quantum dots (multiple exciton generation)[7,8] and dye molecules (singlet fission),[9,10] rare-earth (RE) ion-doped inorganic materials for downconversion have the highest converting efficiency as well as the best physical and chemical stabilities.[11]

Recently, efficient downconversion from visible to NIR has been demonstrated in RE^{3+}-Yb^{3+} (RE = Pr, Tb, Tm) codoped systems,[12−17] where the Yb^{3+} ion is used as acceptor because its two energy levels, $^2F_{7/2}$ and $^2F_{5/2}$, are separated by approximately 10,000 cm^{-1}, matching well with the band gap of crystalline Si. Unfortunately, the absorption of the solar spectrum is very limited since the intraconfigurational parity forbidden 4f → 4f transitions are naturally weak in absorption cross section (about 10^{-21} cm^2) and narrow in absorption bandwidth (sharp lines). To enhance the absorption of the solar spectrum, broadband sensitizers with high absorption cross sections are needed and have been searched extensively. One of the possible strategies is to use organic dyes or quantum dots as the sensitizers,[11,18,19] but dye molecules usually suffer from strong photodegradation and quantum dots have limited quantum efficiency (QE). Another is to codope Ce^{3+} (or Eu^{2+}) into Yb^{3+} activated materials as the allowed 4f → 5d electric-dipole transitions have larger absorption cross section (about 10^{-18} cm^2) and broad absorption band. At first, it was believed that the sensitization of Yb^{3+} by Ce^{3+} is a cooperative energy transfer(ET) process with a theoretical QE as high as 200% since there are no intermediate levels between Ce^{3+} and Yb^{3+} to make the resonant ET impossible. However, up to now, there is no direct evidence of the existence of cooperative process, while the measured QE of Yb^{3+} emission in the codoped samples is well below 100%, indicating that a single-photon downshift process may be involved or even dominant and thus Ce^{4+}-Yb^{2+} charge-transfer (CT) mechanism was proposed by J. Ueda and S. Tanabe.[20] Subsequently, You

Received: August 15, 2018

DOI: 10.1021/acs.inorgchem.8b02304
Inorg. Chem. XXXX, XXX, XXX−XXX

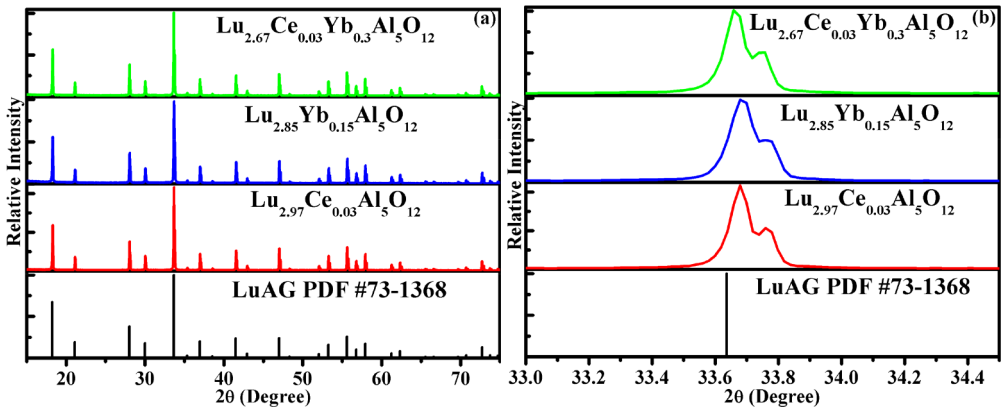

Figure 1. (a) The XRD patterns of Ce^{3+} and/or Yb^{3+}-doped LuAG, the standard pattern of LuAG (PDF #73-1368) are also presented for comparison. (b) The main peak (420) of Ce^{3+} and/or Yb^{3+}-doped LuAG in the range of 33°−34.5°.

et al. further discussed the possible electron-transfer processes using thermoluminescence (TL) spectroscopy to determine the location of energy levels of Ce^{3+} and Yb^{2+} in $Y_3Al_5O_{12}$ (YAG).[21,22] In addition, Yu et al.[23] used the Monte Carlo model to analytically identify the ET processes operative in codoped systems via simulating the decay curves and also concluded that the ET from Ce^{3+} to Yb^{3+} in YAG is a single-step process via Ce^{4+}-Yb^{2+} charge-transfer state (CTS). Nevertheless, direct proof of the Ce^{4+}-Yb^{2+} CT process is still lacking, and several later papers insist on the explanation of the cooperative process, especially at high concentrations of Yb^{3+}.[24−29] It is noteworthy that recently the internal QE of Ce^{3+} and Yb^{3+} codoped perovskite nanocrystals was reported to be as high as 146%, and the enhanced performance of the silicon solar cells was also achieved, though the proposed mechanism is debatable.[29] Besides, Zhou et al. believed that a multiphonon-assisted electric dipole−electric quadrupole mechanism dominates the ET process at a relatively low concentration of Yb^{3+} (≤5 mol %).[30] Hence, the ET mechanism involved in the Ce^{3+}-Yb^{3+} pair is still in dispute.

RE ion-doped $Lu_3Al_5O_{12}$ (LuAG) have been intensively studied for their excellent performance in the fields of scintillators,[31] lasers,[32] and lighting.[33] Recently, Ce^{3+}-doped LuAG (LuAG:Ce^{3+}) has been widely used as green phosphor for white LEDs due to its high QE and good thermal stability.[34,35] As one of the few phosphors that can efficiently absorb blue light, LuAG:Ce^{3+} has short emission in wavelength (peaking at 515 nm) and suffers little thermal quenching compared with Ce^{3+}-doped YAG, both of which are advantageous to spectral conversion from blue to NIR when Yb^{3+} is codoped. Besides, garnet-type materials can be easily made into transparent ceramics owing to their optically isotropic properties, which is a virtue for LuAG as spectral converter. Most importantly, lutetium and ytterbium are next to each other on the periodic table, and thus Lu^{3+} and Yb^{3+} have nearly the same ionic radii, indicating that LuAG can serve as an ideal host for us to investigate the ET mechanism from Ce^{3+} to Yb^{3+}.

In this work, for the first time, we report the visible-to-NIR spectral conversion due to efficient ET from Ce^{3+} to Yb^{3+} in LuAG host via optimizing the doping concentration. Moreover, we systematically reinvestigate the underlying ET mechanism by detailed excitation and emission spectra as well as fluorescent decay curves, and further demonstrate that fast metal-to-metal CT from Ce^{3+} to nearby Yb^{3+} is the dominant ET mechanism. Finally, we provide new experimental evidence that Ce^{4+}-Yb^{2+} CTS is responsible for the relatively low QE of NIR emission in Ce^{3+} and Yb^{3+} codoped system.

EXPERIMENTAL SECTION

Sample Preparation. The powder samples were synthesized by the high-temperature solid-state reaction with raw materials of high-purity Lu_2O_3, CeO_2, Al_2O_3, and Yb_2O_3. They were weighed stoichiometrically according to the composition of $(Lu_{0.99-x}Ce_{0.01}Yb_x)_3Al_5O_{12}$, and 3 wt % AlF_3 was appended as the flux. After thorough mixing in an agate mortar, the resulting mixtures were heated at 1550 °C for 5 h under CO reducing atmosphere. Finally, the samples were cooled to room temperature in the furnace and ground again for the following characterization.

Characterization. The crystal structure of samples were identified by X-ray diffraction (XRD) (Bruker D8 Focus diffractometer, in the 2θ range from 15° to 75° with Cu Kα radiation (λ = 1.54056 Å) operating at 40 kV and 30 mA). X-ray photoelectron spectroscopy (XPS) measurements were conducted by using an ESCALAB 250Xi spectrometer (Thermo Fisher Scientific, USA) with Al Kα radiation as the excitation source. Room-temperature photoluminescence (PL) and photoluminescence excitation (PLE) spectra were measured with FLS920 spectrometer (Edinburgh Instruments, U.K.). A power controllable 980 nm laser diode was used to obtain the PL spectra under NIR excitation. The fluorescence decays of Ce^{3+} were also measured by FLS920 spectrometer with a nanosecond hydrogen flash-lamp (nF900, Edinburgh Instruments) as the excitation source. All the measurements were conducted at room temperature.

RESULTS

The representative XRD patterns of the as-synthesized samples $Lu_{2.97}Ce_{0.03}Al_5O_{12}$, $Lu_{2.85}Yb_{0.15}Al_5O_{12}$, and $Lu_{2.67}Ce_{0.03}Yb_{0.3}Al_5O_{12}$ are shown in Figure 1a. It is obvious that all the diffraction peaks of the samples can be well indexed to the cubic structure of LuAG (PDF #73-1368), and no detectable impurities are presented, indicating the formation of LuAG pure phase. Besides, nearly no shift of the diffraction peaks can be observed with increasing Yb^{3+} concentration, as shown clearly by the partial enlargement of the main peak (420) in Figure 1b, which is due to the very small difference in the ionic radius ($R(Yb^{3+})$ = 0.985 Å and $R(Lu^{3+})$ = 0.977 Å when coordination number is 8).[36] This point is beneficial for us to investigate the ET mechanism, since if large differences exist, the PL properties of the sensitizer Ce^{3+} will be influenced significantly by the regulated local structure in addition to the ET process concerned. To confirm the valence states of Yb element, the XPS measurements of $Lu_{2.7}Yb_{0.3}Al_5O_{12}$ and

DOI: 10.1021/acs.inorgchem.8b02304
Inorg. Chem. XXXX, XXX, XXX−XXX

$Lu_{2.67}Ce_{0.03}Yb_{0.3}Al_5O_{12}$ were conducted (see Figure S1 in the Supporting Information), which was calibrated by using the C 1s peak at 284.6 eV. The XPS spectra indicate the presence of Al, Yb, Lu, and O elements and the appearance of Ce after CeO_2 was added into the raw materials. The two peaks located at 196.43 and 206.50 eV in the enlarged XPS spectrum can be attributed to Lu $4d_{5/2}$ and Lu $4d_{3/2}$, respectively. The Yb^{3+} 4d peak can be clearly observed at 185.3 eV in both of the samples and no detectable peaks or shoulders of Yb^{2+} at 180.3 and 188.8 eV appear when Ce^{3+} is introduced.

As shown in Figure 2a, the PLE spectrum monitored at 515 nm of Ce^{3+} singly doped LuAG exhibits two strong excitation

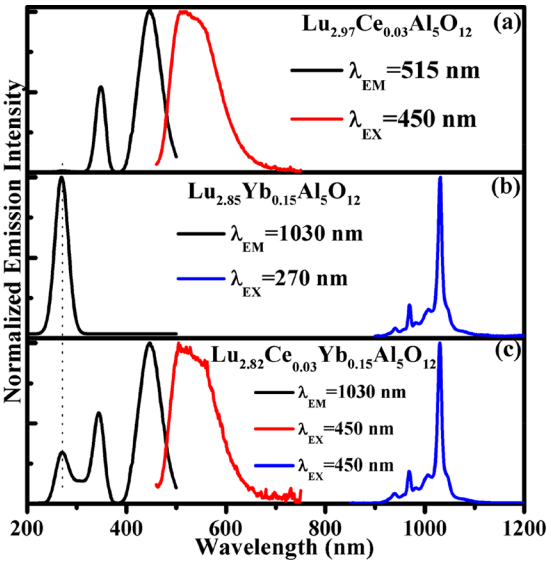

Figure 2. PL and PLE spectra of $Lu_{2.97}Ce_{0.03}Al_5O_{12}$ (a), $Lu_{2.85}Yb_{0.15}Al_5O_{12}$ (b), and $Lu_{2.82}Ce_{0.03}Yb_{0.15}Al_5O_{12}$ (c).

bands peaking at 350 and 450 nm, which are assigned to the 4f−5d transitions of Ce^{3+}. Under 450 nm excitation, the Ce^{3+}-doped LuAG shows intense green emission with an asymmetric emission band peaking at 515 nm, resulting from the transitions of Ce^{3+} from the lowest 5d level to the doublet ground levels ($^2F_{5/2}$ and $^2F_{7/2}$) of the 4f configurations. As for Yb^{3+} singly doped LuAG (Figure 2b), upon UV light (270 nm) excitation, its PL spectrum shows a strong NIR emission lines at 1030 nm originating from the transition of the excited level $^2F_{5/2}$ to the lowest ground level $^2F_{7/2}$ of Yb^{3+}. The PLE spectrum of the Yb^{3+} NIR emission contains a broad excitation band in the UV range of 250−300 nm that is attributed to the ligand (O^{2-}) to metal (Yb^{3+}) CT absorption. The upper level ($^2F_{5/2}$) of Yb^{3+} is separated by 10,000 cm^{-1} from the lower level ($^2F_{7/2}$), which means at least 12 phonons are needed to assist its multiphonon relaxation (the maximum phonon energy is about 800 cm^{-1}), and thus nonradiative relaxation is weak. Besides, the absorption coefficient of Yb^{3+}:$^2F_{7/2} \rightarrow {}^2F_{5/2}$ is relatively large compared with other f−f transitions, which has been widely used as a sensitizer. Therefore, the NIR excitation band resulting from the transition from $^2F_{7/2}$ to $^2F_{5/2}$ of Yb^{3+} should be also strong. It can be seen from Figure 2c that the PLE spectrum for monitoring Yb^{3+} emission at 1030 nm appears the remarkable 5d excitation bands of Ce^{3+} peaking at 350 and 450 nm, which is similar to that of Ce^{3+} emission at 515 nm. Moreover, the PL spectrum contains not only a weak emission band of Ce^{3+} but also several strong NIR emission lines around 1030 nm of Yb^{3+} upon 450 nm excitation. These two features illustrate the occurrence of ET from Ce^{3+} to Yb^{3+} in Ce^{3+} and Yb^{3+} codoped LuAG.

To further illustrate the ET process from Ce^{3+} to Yb^{3+}, the emission intensities of Ce^{3+} and Yb^{3+} as a function of Yb^{3+} concentration were also measured. Figure 3 shows the PL

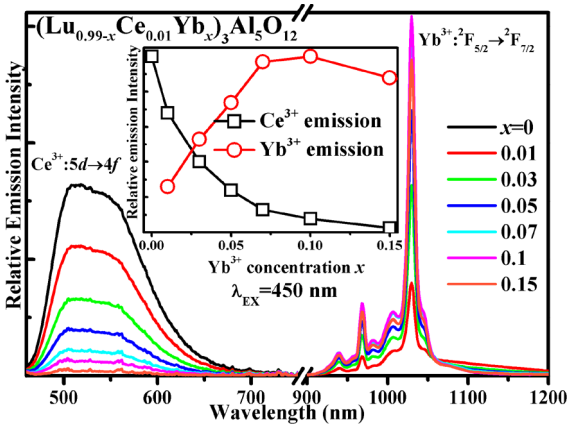

Figure 3. PL spectra of $(Lu_{0.99-x}Ce_{0.01}Yb_x)_3Al_5O_{12}$ (x = 0−0.15) upon excitation to Ce^{3+}:5d level at 450 nm.

spectra of sample series $(Lu_{0.99-x}Ce_{0.01}Yb_x)_3Al_5O_{12}$ (x = 0−0.15) under 450 nm excitation. With increasing the concentration of Yb^{3+}, the NIR emission of Yb^{3+} becomes stronger accompanied by the attenuation of the green emission of Ce^{3+} owing to the enhanced ET from Ce^{3+} to Yb^{3+}. The PL intensity of Yb^{3+} reaches a maximum value at x = 0.1 (see the inset of Figure 3), beyond which it starts to decrease due to the concentration quenching among Yb^{3+} ions; therefore, the optimal Yb^{3+} concentration was determined to be x = 0.1.

Given that the local structure of Ce^{3+} changes little with the replacement of Lu^{3+} by Yb^{3+} and thus its PL intensity is influenced merely by the ET process, the ET efficiency from Ce^{3+} to Yb^{3+}, η_{ET}, can be calculated by

$$\eta_{ET} = 1 - \frac{I}{I_0} \quad (1)$$

where I_0 and I are the PL intensities of Ce^{3+} in the absence and in the presence of Yb^{3+}, respectively. Accordingly, the ET efficiencies were calculated based on the Yb^{3+} concentration dependence of the PL intensity of Ce^{3+} in Figure 3. As listed in Table 1, the ET efficiency becomes larger with increasing Yb^{3+} concentration and reaches as high as 92% at x = 0.1 where the Yb^{3+} emission is at its highest. Such an efficient ET indicates that the introduction of Ce^{3+} enables $(Lu_{1-x}Yb_x)_3Al_5O_{12}$ to absorb blue and UV light efficiently. Figure 4 shows the AM1.5

Table 1. Calculated Energy Transfer Efficiencies of $(Lu_{0.99-x}Ce_{0.01}Yb_x)_3Al_5O_{12}$ (x = 0−0.15)

x	$\eta_{ET} = 1 - I/I_0$ (%)	$\eta_{ET}' = 1 - \tau/\tau_0$ (%)
0	0	0
0.01	0.32	0.18
0.03	0.60	0.25
0.05	0.76	0.37
0.07	0.87	0.47
0.1	0.92	0.51
0.15	0.97	0.58

DOI: 10.1021/acs.inorgchem.8b02304
Inorg. Chem. XXXX, XXX, XXX−XXX

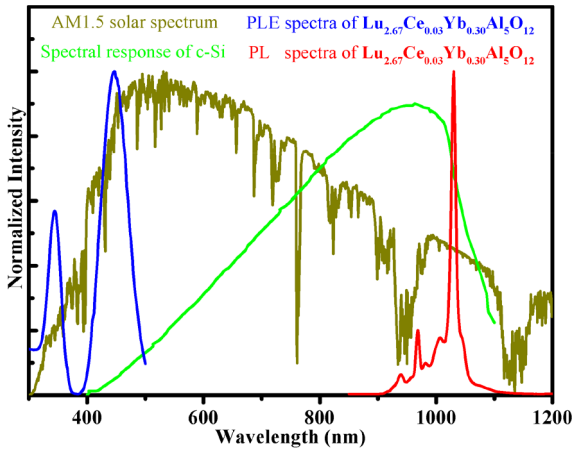

Figure 4. Normalized PLE spectrum of $Lu_{2.67}Ce_{0.03}Yb_{0.30}Al_5O_{12}$ (blue line) and PL spectra of $Lu_{2.67}Ce_{0.03}Yb_{0.30}Al_5O_{12}$ (red line). AM 1.5 G solar spectrum (dark yellow line) and spectral response of c-Si (green line) are the background.

solar spectrum in the range of 300−1200 nm and the response of the Si solar cell compared with the excitation and emission spectra of $Lu_{2.67}Ce_{0.03}Yb_{0.30}Al_5O_{12}$. The PLE spectra of Ce^{3+} in the blue and UV spectral range from 300 to 500 nm agree with the maximum intensity of the solar spectrum, which makes an additional 10% of solar power. Besides, Yb^{3+} gives an intense NIR emission around 1030 nm, which matches well with the highest spectral response of c-Si solar cells. Therefore, $Lu_{2.67}Ce_{0.03}Yb_{0.30}Al_5O_{12}$ has the potential to be used as spectral converter for c-Si solar cells, especially considering that LuAG host can be made into transparent ceramics with relatively large size.[37,38]

However, one may notice that on the codoping of Yb^{3+}, the emission intensity of Ce^{3+} also exhibits a strong quenching, while that of Yb^{3+} increases little in LuAG. To confirm the ET from Ce^{3+} to Yb^{3+}, we measured the decay curves of Ce^{3+} 5d−4f emission (515 nm) of $(Lu_{0.99-x}Ce_{0.01}Yb_x)_3Al_5O_{12}$ (x = 0−0.15) under 450 nm excitation. It can be seen from Figure 5 that the decay curve of Ce^{3+} deviates from the single exponential profile with the introduction of Yb^{3+} and becomes steeper and steeper with increasing its concentration, indicating the occurrence of nonradiative ET from Ce^{3+} to Yb^{3+}. The effective lifetime of Ce^{3+} is defined as

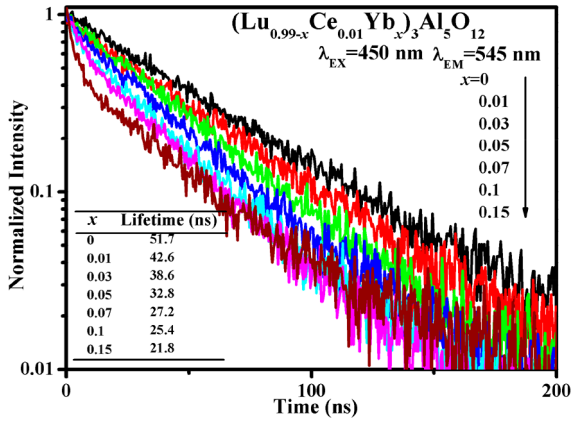

Figure 5. Fluorescent decay curves of Ce^{3+}:5d level in $(Lu_{0.99-x}Ce_{0.01}Yb_x)_3Al_5O_{12}$ (x = 0−0.15) upon excitation at 450 nm.

$$\tau = \frac{\int_0^\infty tI(t)dt}{\int_0^\infty I(t)dt} \quad (2)$$

where the $I(t)$ is the intensity at time t. As shown in Figure 5, the effective lifetime decreases monotonically with Yb^{3+} concentration, which confirms the ET from Ce^{3+} to Yb^{3+}. The ET efficiency η_{ET}' from Ce^{3+} to Yb^{3+} can be calculated by the following equation:

$$\eta_{ET}' = 1 - \frac{\tau}{\tau_0} \quad (3)$$

where τ_0 and τ are the lifetimes of Ce^{3+} in the presence and in the absence of Yb^{3+}, respectively. The calculated ET efficiencies from Ce^{3+} to Yb^{3+} using eq 3 are also listed in Table 1, and η_{ET}' reaches 51% for Yb^{3+} concentration at x = 0.1. One may notice that the values calculated by eq 3 are apparently smaller than those calculated by eq 1, which can be well explained by the existence of fast ET process from Ce^{3+} to its nearby Yb^{3+} and will be further discussed in the following part.

DISCUSSION

As discussed by several previous papers, one of the most controversial issues is that if it is a cooperative downconversion (quantum cutting) process or just a downshifting (single-photon) process for ET from Ce^{3+} to Yb^{3+} (see Figure 6).

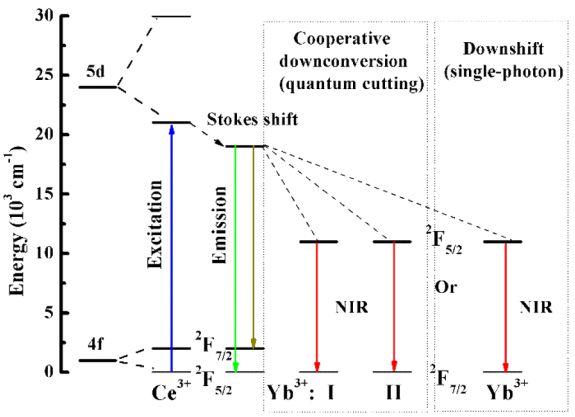

Figure 6. Schematic energy level diagrams of Ce^{3+} and Yb^{3+} with the involved ET process.

According to the model proposed by Dorenbos, Yu et al.[23] concluded that the $5d_1$ state of Ce^{3+} is generally higher in energy than the ground state of Yb^{2+}, and thus charge transfer from the $5d_1$ state of Ce^{3+} to Yb^{3+} is energetically favorable in any host, which is agreed with the experimental results of TL spectroscopy reported by You et al.[21,22] Besides, through comparison of the simulated decay curves of Ce^{3+} $5d_1 \rightarrow 4f$ emission with the measured decay traces, Yu et al.[23] also revealed that ET from Ce^{3+} to Yb^{3+} is just a single-photon ET process via a Ce^{4+}-Yb^{2+} CTS, rather than cooperative downconversion process. As Yu et al. have discussed, their simulations are not perfect and deviations exist between experiment and model, which have been attributed to the energy migration (EM) among Ce^{3+} donors. It is well-known that nonradiative ET from the excited donor (Ce^{3+}) directly to an acceptor (Yb^{3+}) is a short-range process, which occurs within the interionic distance of about 20 Å for electric

DOI: 10.1021/acs.inorgchem.8b02304
Inorg. Chem. XXXX, XXX, XXX−XXX

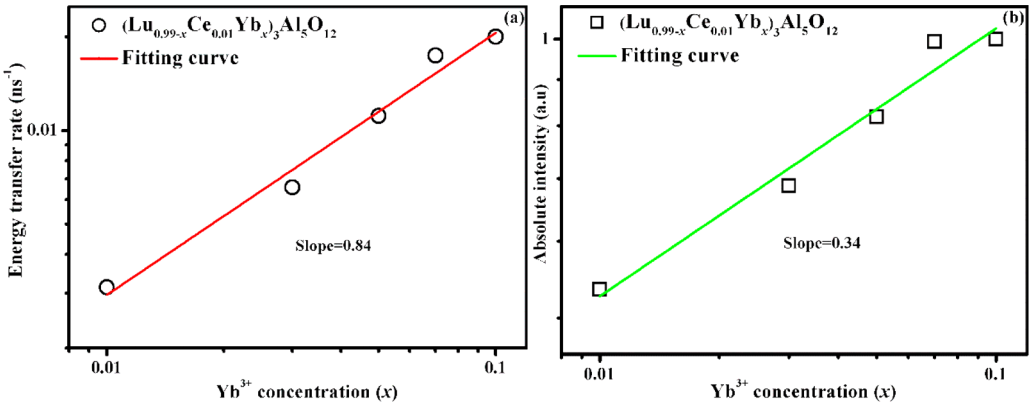

Figure 7. (a) Plot (log–log) of the ET rate versus the Yb^{3+} concentration in $(Lu_{0.99-x}Ce_{0.01}Yb_x)_3Al_5O_{12}$ (x = 0.01–0.1). (b) Plot (log–log) of the integrated PL intensity of Yb^{3+} versus the Yb^{3+} concentration in $(Lu_{0.99-x}Ce_{0.01}Yb_x)_3Al_5O_{12}$ (x = 0.01–0.1).

dipole–dipole interaction or much shorter for electric dipole–quadrupole interaction and exchange interaction, while ET from the excited donor (Ce^{3+}) to another unexcited donor (still Ce^{3+}), named EM, can allow the energy of the excited Ce^{3+} to reach much further acceptor (Yb^{3+}) by successive ET among several or even many donors (i.e., EM) and finally to an acceptor (Yb^{3+}). Such EM process may be responsible for the electric dipole–quadrupole mechanism proposed by Zhou et al., since the concentration of Ce^{3+} is as high as 3.33 mol % in their case where the donor-to-donor EM process may be pronounced.[30] It should be noted that the Inokuti–Hirayama expression and the modified one are applicable only when the EM process is too weak to be negligible,[23,39] because if the EM process is dominant over ET process, a less distance-dependent mechanism will be concluded by the Inokuti–Hirayama model.

The measurement of decay curve has been well accepted to discuss the ET process. For the isolated emitting center, its decay curve is rigorously exponential, so that the overall decay curve can be well linearly fitted in semilogarithmic coordinates with a decay rate of k^0. However, if there exists ET and/or EM processes between different centers, the decay curves will become complicated and are no longer straight lines due to different decay rates. Theoretically, in this case, the overall decay curve of the donor can be divided into two parts with different physical meanings: the initial nonexponential part of the decay curve represents the PL dynamics of donors having at least one acceptor within the interaction range, and the nonexponential feature results from the direct ET from donors to acceptors with various ET rates due to different interionic distances; the exponential tail means that for sufficiently long times, all of the donors having acceptors within interaction range are relaxed so that the decay becomes exponential with time and with a decay rate equal to that of the isolated ion (i.e., k^0), and if the donor–donor EM process exists, the exponential tail will be characterized by a decay rate $k_t = k^0 + k_M$, where k_M represents the contribution of the donor–donor EM process to the donor–acceptor ET.[40,41] Considering the above basic physical meanings, we will fully utilize the initial part and the tail of the decay curve separately in our following discussion.

According to our previous work, for a cooperative ET process, the ET rate (W_{coop}) should be quadratically dependent on Yb^{3+} ion concentration (x),[13,42] i.e., $W_{coop} = Cx^2$, where C represents the ET coefficient, since one Ce^{3+} ion transfers its excitation energy simultaneously to two nearby Yb^{3+}ions. For a single-photon ET process, however, the ET process from Ce^{3+} to Yb^{3+} is one-to-one, and thus the ET rate (W_{single}) should be proportional to Yb^{3+} ion concentration, simply written as $W_{single} = C'x$. To identify the possible ET routes, the dependence of the ET rate upon Yb^{3+} concentration was analyzed. The ET rate can be obtained by

$$W = \frac{1}{\tau} - \frac{1}{\tau_0} \tag{4}$$

As discussed above, the ET rate can be extracted only from the initial parts of the decay curves because the EM process usually exists. Accordingly, the average lifetime (τ) of Ce^{3+} in the codoped samples was calculated based on the initial parts of the corresponding decay curves at this point. The calculated values of the ET rate (W) as a function of Yb^{3+} concentration (x) are plotted in a double-logarithmic diagram, as shown in Figure 7a. The slope is fitted to be 0.84, indicating the ET from Ce^{3+} to Yb^{3+} in LuAG is dominated by the single-photon ET process rather than the cooperative one. Moreover, from the perspective of Yb^{3+}, the cooperative ET process requires two Yb^{3+} ions to be close to the same Ce^{3+} ion, so that the PL intensity of Yb^{3+} should increase as the square of the Yb^{3+} concentration if the cooperative ET process is the principal one for sensitizing Yb^{3+}, at least for relatively low Yb^{3+} concentrations.[43,44] As shown in Figure 7b, the dependence of the integrated PL intensity of Yb^{3+} on its concentration is fitted with the slope of only 0.34 in a double-logarithmic diagram, which is much smaller than 2. Therefore, we come to the unambiguous conclusion that the ET from Ce^{3+} to Yb^{3+} occurs via a single-photon process.

As mentioned before (see Table 1), there is a large difference between the ET efficiencies calculated by eqs 1 and 3, respectively, which is a common feature in the Ce^{3+}-Yb^{3+} systems[42,45,46] and has been found in other codoped systems, such as Ce^{3+}-Tb^{3+},[47,48] Ce^{3+}-Mn^{2+},[49] and Nd^{3+}-Er^{3+}.[50] This phenomenon can be well explained by the existence of two different types of Ce^{3+} ions. One type of Ce^{3+} has at least one Yb^{3+} as nearest neighbor, whereas the other has none. These Ce^{3+} having nearest-neighbor Yb^{3+} will decay extremely fast due to very large ET rates (much larger than their radiative rates) to Yb^{3+}, so that their emission is quenched without luminescence detected, leading to the absence of the fast initial part in the decay curve of Ce^{3+}. On the other hand, those Ce^{3+} having no nearest-neighbor Yb^{3+} will practically radiate all the excitation energy. Thus, the calculated effective lifetimes of Ce^{3+} appears to be reduced less than the real ones as Yb^{3+} is

DOI: 10.1021/acs.inorgchem.8b02304
Inorg. Chem. XXXX, XXX, XXX–XXX

codoped, resulting in the smaller ET efficiencies.[47−49] Note that the finite rise time of the detection system (about 0.5 ns) leads to our failure to observe the very early fluorescence data in our decay curve measurement,[23,50] and a more sophisticated instrument is needed to obtain the overall decay curve, which is beneficial for us to discuss the detailed ET mechanism. The existence of fast ET process indicates that the dominant ET mechanism is a short-range interaction and strongly dependent on the interionic distance, such as the exchange interaction, the electron transfer, and the electric dipole−quadrupole or higher-order interaction.[23,30,47] The exchange interaction can be readily excluded since there is no spectral overlap between the Ce^{3+} emission and Yb^{3+} absorption. For the same reason, the electric dipole−quadrupole proposed by Zhou et al. should be negligible, whose results are also unreasonable since the Ce^{3+}−Ce^{3+} EM process is already detectable in our case, as demonstrated by the somewhat steeper exponential tail of the decay curve (see Figure 8). As a result, we believe that the ET

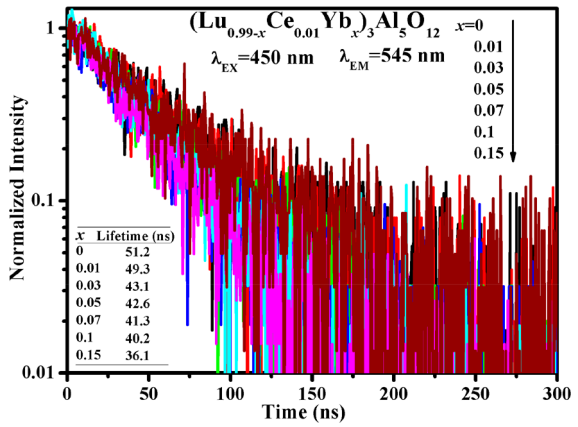

Figure 8. Tail of the fluorescent decay curves of Ce^{3+}:5d level in $(Lu_{0.99-x}Ce_{0.01}Yb_x)_3Al_5O_{12}$ (x = 0−0.15) upon excitation at 450 nm.

from Ce^{3+} to Yb^{3+} is an electron-transfer process via Ce^{4+}-Yb^{2+} CTS, whose ET rate is exponentially dependent on the donor−acceptor distance as that of the exchange interaction because electron transfer involves wave function overlap.

As schematically depicted in Figure 9, the above metal-to-metal (Ce^{3+}-to-Yb^{3+}) electron transfer in LuAG can be explained by a configuration coordinate model proposed by Yu et al.[23] The Ce^{4+}-Yb^{2+} CTS can be easily formed even at low temperature with a small activation barrier E_1 after the

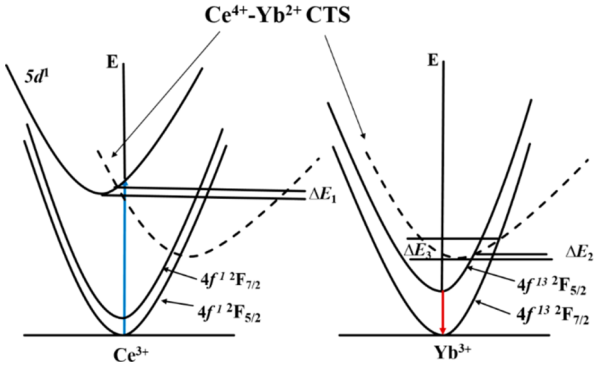

Figure 9. Simplified configurational coordinate diagram of the excited and ground states of Ce^{3+} and Yb^{3+}.

excitation of Ce^{3+} 5d state by blue or UV light. The resulted Ce^{4+}-Yb^{2+} pair is much more stable than all its excited states, and the associated level lies between the Ce^{3+}-Yb^{3+} states, which involves in the ET from Ce^{3+} to Yb^{3+} as well as in the quenching of Yb^{3+} emission after the excitation of Ce^{3+}.[51] The Ce^{4}+-Yb^{2+} CTS has two possible decay pathways: The first is the transition of Ce^{4+}-Yb^{2+} CTS to $Ce^{3+}(4f^1)$-$Yb^{3+}(^2F_{5/2})$ with an activation barrier E_2, where Yb^{3+} is excited into $^2F_{5/2}$ state followed by emitting a NIR photon ($^2F_{5/2}$-$^2F_{7/2}$); the second is the transition of Ce^{4+}-Yb^{2+} CTS to $Ce^{3+}(4f^1)$-$Yb^{3+}(^2F_{7/2})$ with an activation barrier E_3, which means Yb^{3+} reaches the ground $^2F_{7/2}$ state nonradiatively, resulting in no Yb^{3+} NIR emission.[23]

Ueda and Tanabe demonstrated in Ce^{3+} and Yb^{3+} codoped YAG that the internal QE of Yb^{3+} NIR emission is only about 10% upon Ce^{3+} excitation by blue light, but as high as 80% upon direct Yb^{3+} excitation by NIR light.[20] This has been explained by quantitatively analyzing the configuration coordinate diagrams that both of the Yb^{2+}-Yb^{3+} pair and the Ce^{4+}-Yb^{2+} CTS are responsible for the quenching of Yb^{3+} emission.[51] To confirm the influence of Ce^{4+}-Yb^{2+} CTS experimentally, we measured the PL intensities of Yb^{3+} NIR emission as a function of Ce^{3+} concentration upon Yb^{3+}-O^{2-} CT excitation and direct $^2F_{7/2}$-$^2F_{5/2}$ excitation, respectively. As shown in Figure 10a, the CT excitation band of Yb^{3+} peaking at 270 nm declines remarkably as Ce^{3+} is introduced into $Lu_{2.7}Yb_{0.3}Al_5O_{12}$ accompanied by the appearance of the excitation band of Ce^{3+}. Nonetheless, when the 980 nm laser was used to directly excite the $Yb^{3+2}F_{5/2}$ level, the decrease of NIR emission is very small (9%) with the increase of Ce^{3+} concentration (see Figure 10b). Two factors are included to explain such a small influence of Ce^{3+} on the luminescence properties of Yb^{3+} upon direct $Yb^{3+2}F_{7/2}$-$^2F_{5/2}$ excitation: One is Yb^{3+} can transfer its energy to the ground sublevel $^2F_{7/2}$ of Ce^{3+} with the assistance of phonons, and considering the large energy mismatch (about ten phonons needed), it is reasonable to conclude that the nonradiative phonon-assisted cross relaxation of the $Yb^{3+2}F_{5/2}$ state by Ce^{3+} ($^2F_{7/2}$-$^2F_{5/2}$) is negligible;[52] and the other one comes from the difference of radii between Ce^{3+} and Lu^{3+}, which may affect the crystal lattice, and this influence is also limited because of the low doping content of Ce^{3+} (only 1 mol %). This result gives the experimental evidence of the Ce^{4+}-Yb^{2+} CTS in quenching the Yb^{3+} NIR emission. Specifically, Yb^{3+}-O^{2-} CT excitation will lead to the production of Yb^{2+}, and thus the nonradiative crossover in Yb^{2+}/Yb^{3+} mixed valence pair will quench the Yb^{3+} NIR emission, which is the only nonradiative decay pathway in the absence of Ce^{3+}.[51] In the presence of Ce^{3+}, however, the existence of Ce^{4+}-Yb^{2+} CTS will provide an additional quenching pathway, which is reflected by the obvious decrease of the CT excitation band. Such a large reduction (76%) can explain why the measured internal QE of Yb^{3+} NIR emission in Ce^{3+}-Yb^{3+} system is only about 10%, which also demonstrates experimentally that the ET from Ce^{3+} to Yb^{3+} is a single-photon process via Ce^{4+}-Yb^{2+} CTS. Finally, it is noteworthy that the ET can be dominated by the multipolar interaction in lightly doped samples if there is spectral overlap between the emission of the donor and the $^2F_{7/2}$-$^2F_{5/2}$ excitation of Yb^{3+}, which has been demonstrated by Zhou et al. in Eu^{2+} and Yb^{3+} codoped $Ca_3Sc_2Si_3O_{12}$.[53] However, if there is no spectral overlap (such as in our work) and there exists a large energy gap between Ce^{3+}/Eu^{2+} and Yb^{3+}, the occurrence of ET will need the assistance of at least five phonons, so that the

DOI: 10.1021/acs.inorgchem.8b02304
Inorg. Chem. XXXX, XXX, XXX−XXX

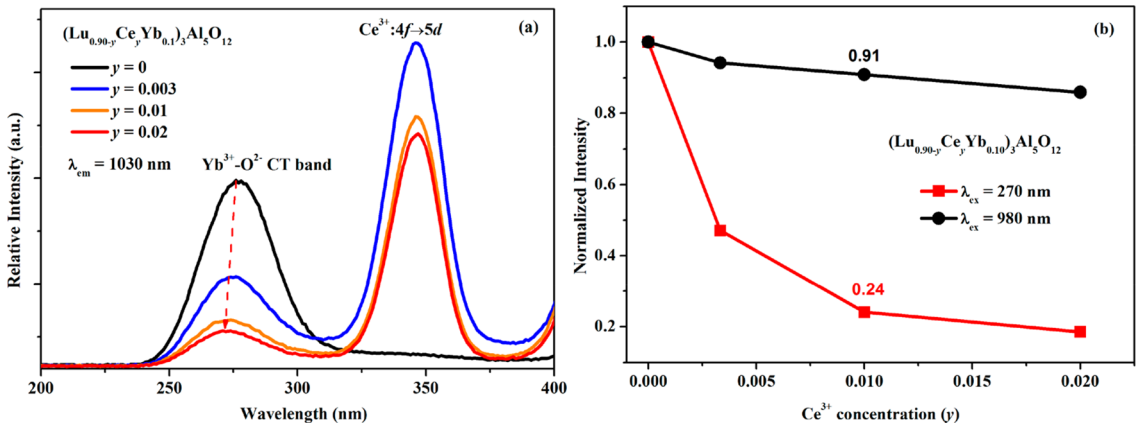

Figure 10. (a) The PLE spectra of $(Lu_{0.9-y}Ce_yYb_{0.1})_3Al_5O_{12}$ (y = 0−0.02) monitored at 1030 nm. (b) The normalized PL intensities of Yb^{3+} NIR emission as a function of Ce^{3+} concentration in $(Lu_{0.9-y}Ce_yYb_{0.1})_3Al_5O_{12}$ (y = 0−0.02) upon Yb^{3+}-O^{2-} CT excitation and direct $^2F_{7/2}$-$^2F_{5/2}$ excitation, respectively.

probability of the ET from Ce^{3+}/Eu^{2+} to Yb^{3+} due to the multipolar interaction will be extremely low.

CONCLUSIONS

In summary, we demonstrate the efficient visible-to-NIR spectral conversion in Ce^{3+} and Yb^{3+} codoped LuAG with the ET efficiency as high as 92% for the doping concentration optimized sample $Lu_{2.67}Ce_{0.03}Yb_{0.30}Al_5O_{12}$. The underlying ET mechanism from Ce^{3+} to Yb^{3+} was systematically re-investigated by the detailed excitation and emission spectra as well as fluorescent decay curves, especially utilizing the initial part and the tail of the decay curve separately. Our results show that fast metal-to-metal CT from Ce^{3+} to nearby Yb^{3+} is the dominant ET mechanism, thus indicating that it is just a single-photon process for ET from Ce^{3+} to Yb^{3+}. Moreover, a marked drop in the Yb^{3+}-O^{2-} CT excitation band with the introduction of Ce^{3+} proves the existence of Ce^{4+}-Yb^{2+} CTS experimentally, which also well explains the relatively low measured internal QE of Yb^{3+} NIR emission in Ce^{3+}-Yb^{3+} system. Finally, it should be remarked that for practical application, the QE of NIR Yb^{3+} emissions should be largely enhanced by separating them in space to minimize the Ce^{3+} to Yb^{3+} CT process, such as introducing Tb^{3+} or Pr^{3+} as the bridge ion[54,55] and constructing a core−shell structure,[56] which needs work in the future.

ASSOCIATED CONTENT

Supporting Information

The Supporting Information is available free of charge on the ACS Publications website at DOI: 10.1021/acs.inorgchem.8b02304.

Figure S1 (PDF)

AUTHOR INFORMATION

Corresponding Authors

*E-mail: wengsee@163.com.

*E-mail: zhangjh@ciomp.ac.cn.

ORCID

Dan Wu: 0000-0001-8411-6737

Wenge Xiao: 0000-0002-3719-9434

Notes

The authors declare no competing financial interest.

ACKNOWLEDGMENTS

This work was partially supported by the Program of Higher-Level Talents of Inner Mongolia University (grant no. 5185108), National Key Research and Development Program of China (grant no. 2016YFB0701003, 2016YFB0400605), and National Natural Science Foundation of China (grant no. 61275055, 11274007).

REFERENCES

(1) Shockley, W.; Queisser, H. J. Detailed Balance Limit of Efficiency of p-n Junction Solar Cells. *J. Appl. Phys.* **1961**, *32*, 510−519.

(2) Polman, A.; Knight, M.; Garnett, E. C.; Ehrler, B.; Sinke, W. C. Photovoltaic Materials: Present Efficiencies and Future Challenges. *Science* **2016**, *352*, aad4424.

(3) Huang, X.; Han, S.; Huang, W.; Liu, X. Enhancing Solar Cell Efficiency: the Search for Luminescent Materials as Spectral Converters. *Chem. Soc. Rev.* **2013**, *42*, 173−201.

(4) Van Der Ende, B. M.; Aarts, L.; Meijerink, A. Near-Infrared Quantum Cutting for Photovoltaics. *Adv. Mater.* **2009**, *21*, 3073−3077.

(5) Wang, X.; Yan, X.; Kan, C. Controlled Synthesis and Optical Characterization of Multifunctional Ordered Y_2O_3: Er^{3+} Porous Pyramid Arrays. *J. Mater. Chem.* **2011**, *21*, 4251−4256.

(6) Lee, J.; Yoo, B.; Lee, H.; Cha, G. D.; Lee, H. S.; Cho, Y.; Kim, S. Y.; Seo, H.; Lee, W.; Son, D.; Kang, M.; Kim, H. M.; Park, Y.; Hyeon, T.; Kim, D. H. Ultra-Wideband Multi-Dye-Sensitized Upconverting Nanoparticles for Information Security Application. *Adv. Mater.* **2017**, *29*, 1603169.

(7) Kagan, C. R.; Lifshitz, E.; Sargent, E. H.; Talapin, D. V. Building Devices from Colloidal Quantum Dots. *Science* **2016**, *353*, aac5523.

(8) Makarov, N. S.; Guo, S.; Isaienko, O.; Liu, W.; Robel, I.; Klimov, V. I. Spectral and Dynamical Properties of Single Excitons, Biexcitons, and Trions in Cesium−Lead-Halide Perovskite Quantum Dots. *Nano Lett.* **2016**, *16*, 2349−2362.

(9) Smith, M. B.; Michl, J. Singlet Fission. *Chem. Rev.* **2010**, *110*, 6891−6936.

(10) Basham, J. I.; Mor, G. K.; Grimes, C. A. Förster Resonance Energy Transfer in Dye-Sensitized Solar Cells. *ACS Nano* **2010**, *4*, 1253−1258.

(11) Wang, Z.; Meijerink, A. Dye-sensitized Downconversion. *J. Phys. Chem. Lett.* **2018**, *9*, 1522−1526.

(12) Xu, Y. S.; Huang, F.; Fan, B.; Lin, C. G.; Dai, S. X.; Chen, L. Y.; Nie, Q. H.; Ma, H. L.; Zhang, X. H. Quantum Cutting in Pr^{3+}-Yb^{3+} Codoped Chalcohalide Glasses for High-Efficiency c-Si Solar Cells. *Opt. Lett.* **2014**, *39*, 2225−2228.

DOI: 10.1021/acs.inorgchem.8b02304
Inorg. Chem. XXXX, XXX, XXX−XXX

(13) Xiang, G.; Zhang, J.; Hao, Z.; Zhang, X.; Pan, G.; Luo, Y.; Lu, S.; Zhao, H. The Energy Transfer Mechanism in Pr^{3+} and Yb^{3+} Codoped β-$NaLuF_4$ Nanocrystals. *Phys. Chem. Chem. Phys.* **2014**, *16*, 9289−9293.
(14) Vergeer, P.; Vlugt, T. J. H.; Kox, M. H. F.; den Hertog, M. I.; van der Eerden, J. P. J. M.; Meijerink, A. Quantum Cutting by Cooperative Energy Transfer in $Yb_xY_{1-x}PO_4$: Tb^{3+}. *Phys. Rev. B: Condens. Matter Mater. Phys.* **2005**, *71*, No. 014119.
(15) Bouajaj, A.; Belmokhtar, S.; Britel, M. R.; Armellini, C.; Boulard, B.; Belluomo, F.; Di Stefano, A.; Polizzi, S.; Lukowiak, A.; Ferrari, M.; Enrichi, F. Tb^{3+}/Yb^{3+} Codoped Silica−Hafnia Glass and Glass−Ceramic Waveguides to Improve the Efficiency of Photovoltaic Solar Cells. *Opt. Mater.* **2016**, *52*, 62−68.
(16) Zhang, Q. Y.; Yang, G. F.; Jiang, Z. H. Cooperative Downconversion in $GdAl_3(BO_3)_4$: RE^{3+}, Yb^{3+}(RE= Pr, Tb, and Tm). *Appl. Phys. Lett.* **2007**, *91*, No. 051903.
(17) Li, J.; Zhang, J.; Zhang, X.; Hao, Z.; Luo, Y. Cooperative Downconversion and Near Infrared Luminescence of Tm^{3+}/Yb^{3+} Codoped Calcium Scandate Phosphor. *J. Alloys Compd.* **2014**, *583*, 96−99.
(18) Shao, W.; Lim, C. K.; Li, Q.; Swihart, M. T.; Prasad, P. N. Dramatic Enhancement of Quantum Cutting in Lanthanide-Doped Nanocrystals Photosensitized with an Aggregation Induced Enhanced Emission Dye. *Nano Lett.* **2018**, *18*, 4922−4926.
(19) Swabeck, J. K.; Fischer, S.; Bronstein, N. D.; Alivisatos, A. P. Broadband Sensitization of Lanthanide Emission with Indium Phosphide Quantum Dots for Visible to NIR Downshifting. *J. Am. Chem. Soc.* **2018**, *140*, 9120−9126.
(20) Ueda, J.; Tanabe, S. Visible to Near Infrared Conversion in Ce^{3+}-Yb^{3+} Co-Doped YAG Ceramics. *J. Appl. Phys.* **2009**, *106*, No. 043101.
(21) You, F.; Bos, A. J.; Shi, Q.; Huang, S.; Dorenbos, P. Electron Transfer Process Between Ce^{3+} Donor and Yb^{3+} Acceptor Levels in the Bandgap of $Y_3Al_5O_{12}$ (YAG). *J. Phys.: Condens. Matter* **2011**, *23*, 215502.
(22) You, F.; Bos, A. J. J.; Shi, Q.; Huang, S.; Dorenbos, P. Thermoluminescence Investigation of Donor (Ce^{3+}, Pr^{3+}, Tb^{3+}) Acceptor (Eu^{3+}, Yb^{3+}) Pairs in $Y_3Al_5O_{12}$. *Phys. Rev. B* **2012**, *85*, 141−143.
(23) Yu, D. C.; Rabouw, F. T.; Boon, W. Q.; Kieboom, T.; Ye, S.; Zhang, Q. Y.; Meijerink, A. Insights Into the Energy Transfer Mechanism in Ce^{3+}-Yb^{3+} Codoped YAG Phosphors. *Phys. Rev. B: Condens. Matter Mater. Phys.* **2014**, *90*, 165126.
(24) Wang, Q.; Qiu, J.; Song, Z.; Yang, Z.; Yin, Z.; Zhou, D.; Wang, S. NIR Enhancement Based on Energy Transfer Process of Ce^{3+}-Yb^{3+} in Inverse Opal Photonic Crystals. *J. Am. Ceram. Soc.* **2016**, *99*, 911−916.
(25) Luo, Z. H.; Liu, Y. F.; Zhang, C. H.; Zhang, J. X.; Qin, H. M.; Jiang, H. C.; Jiang, J. Effect of Yb^{3+} on the Crystal Structural Modification and Photoluminescence Properties of GGAG: Ce^{3+}. *Inorg. Chem.* **2016**, *55*, 3040−3046.
(26) Hao, Y.; Wang, Y.; Hu, X.; Liu, X.; Liu, E.; Fan, J.; Miao, H.; Sun, Q. YBO_3: Ce^{3+}, Yb^{3+} Based Near-Infrared Quantum Cutting Phosphors: Synthesis and Application to Solar Cells. *Ceram. Int.* **2016**, *42*, 9396−9401.
(27) Liu, X.; Hu, X.; Miao, H.; Zhang, G.; Mu, J.; Han, T.; Zhang, D. CaF_2: Ce^{3+}/Yb^{3+} Hollow Spheres Luminescence Downconversion Property Optimize Anti-Reflective Coatings for Solar Cells. *Sol. Energy* **2016**, *134*, 45−51.
(28) Lin, H.; Zhou, S.; Teng, H.; Li, Y.; Li, W.; Hou, X.; Jia, T. Near Infrared Quantum Cutting in Heavy Yb Doped $Ce_{0.03}Yb_{3x}Y_{(2.97-3x)}Al_5O_{12}$ Transparent Ceramics for Crystalline Silicon Solar Cells. *J. Appl. Phys.* **2010**, *107*, No. 043107.
(29) Zhou, D.; Liu, D.; Pan, G.; Chen, X.; Li, D.; Xu, W.; Bai, X.; Song, H. Cerium and Ytterbium Codoped Halide Perovskite Quantum Dots: a Novel and Efficient Downconverter for Improving the Performance of Silicon Solar Cells. *Adv. Mater.* **2017**, *29*, 1704149.
(30) Zhou, L.; Tanner, P. A.; Ning, L.; Zhou, W.; Liang, H.; Zheng, L. Spectral Properties and Energy Transfer between Ce^{3+} and Yb^{3+} in the $Ca_3Sc_2Si_3O_{12}$ Host: is it an Electron Transfer Mechanism? *J. Phys. Chem. A* **2016**, *120*, 5539−5548.
(31) Ogiegło, J. M.; Zych, A.; Ivanovskikh, K. V.; Justel, T.; Ronda, C. R.; Meijerink, A. Luminescence and Energy Transfer in $Lu_3Al_5O_{12}$ Scintillators Co-Doped with Ce^{3+} and Tb^{3+}. *J. Phys. Chem. A* **2012**, *116*, 8464−8474.
(32) Dong, J.; Ueda, K.; Kaminskii, A. A. Efficient Passively Q-Switched Yb: LuAG Microchip Laser. *Opt. Lett.* **2007**, *32*, 3266−3268.
(33) Setlur, A. A.; Srivastava, A. M. On the Relationship between Emission Color and Ce^{3+} Concentration in Garnet Phosphors. *Opt. Mater.* **2007**, *29*, 1647−1652.
(34) Wu, D.; Hao, Z.; Zhang, X.; Pan, G. H.; Luo, Y.; Zhang, L.; Zhao, H.; Zhang, J. Efficient Energy Back Transfer from Ce^{3+} 5d State to $Pr^{3+1}D_2$ Level in $Lu_3Al_5O_{12}$ upon Pr^{3+} 4f5d Excitation. *J. Lumin.* **2017**, *186*, 170−174.
(35) Xiang, R.; Liang, X.; Li, P.; Di, X.; Xiang, W. A Thermally Stable Warm WLED Obtained by Screen-Printing a Red Phosphor Layer on the LuAG: Ce^{3+} PiG Substrate. *Chem. Eng. J.* **2016**, *306*, 858−865.
(36) Zorenko, Y.; Gorbenko, V. Growth Peculiarities of the $R_3Al_5O_{12}$ (R= Lu, Yb, Tb, Eu-Y) Single Crystalline Film Phosphors by Liquid Phase Epitaxy. *Radiat. Meas.* **2007**, *42*, 907−910.
(37) Xu, J.; Shi, Y.; Xie, J.; Lei, F. Fabrication, Microstructure, and Luminescent Properties of Ce^{3+}-Doped $Lu_3Al_5O_{12}$ (Ce: LuAG) Transparent Ceramics by Low-Temperature Vacuum Sintering. *J. Am. Ceram. Soc.* **2013**, *96*, 1930−1936.
(38) Li, J.; Sahi, S.; Groza, M.; Pan, Y.; Burger, A.; Kenarangui, R.; Chen, W. Optical and Scintillation Properties of Ce^{3+}-Doped LuAG and YAG Transparent Ceramics: A Comparative Study. *J. Am. Ceram. Soc.* **2017**, *100*, 150−156.
(39) Shanmugavelu, B.; Kumar, V. R. K. Luminescence Studies of Dy^{3+} Doped Bismuth Zinc Borate Glasses. *J. Lumin.* **2014**, *146*, 358−363.
(40) Bettinelli, M.; Flint, C. D. Energy Migration and Transfer in the $^5D_0$ State of $Cs_2NaEuCl_6$. *J. Phys.: Condens. Matter* **1991**, *3*, 7053.
(41) Bettinelli, M.; Flint, C. D. Energy Transfer from the $^5D_1$ State of $Cs_2NaY_{1-x}Eu_xCl_6$ and $Cs_2NaEuCl_6$. *J. Phys.: Condens. Matter* **1991**, *3*, 4433.
(42) Li, J.; Chen, L.; Hao, Z.; Zhang, X.; Zhang, L.; Luo, Y.; Zhang, J. Efficient Near-Infrared Downconversion and Energy Transfer Mechanism of Ce^{3+}/Yb^{3+} Codoped Calcium Scandate Phosphor. *Inorg. Chem.* **2015**, *54*, 4806−4810.
(43) DeLuca, J. A.; Ham, F. S. Efficient Luminescent Energy Transfer from Mn^{2+} to Yb^{3+} in CaF_2. *J. Electrochem. Soc.* **1977**, *124*, 1592−1598.
(44) Yuan, J. L.; Zeng, X. Y.; Zhao, J. T.; Zhang, Z. J.; Chen, H. H.; Yang, X. X. Energy Transfer Mechanisms in Tb^{3+}, Yb^{3+} Codoped Y_2O_3 Downconversion Phosphor. *J. Phys. D: Appl. Phys.* **2008**, *41*, 105406.
(45) Sontakke, A. D.; Ueda, J.; Katayama, Y.; Zhuang, Y.; Dorenbos, P.; Tanabe, S. Role of Electron Transfer in Ce^{3+} Sensitized Yb^{3+} Luminescence in Borate Glass. *J. Appl. Phys.* **2015**, *117*, No. 013105.
(46) Zhang, H.; Liu, X.; Zhao, F.; Zhang, L.; Zhang, Y.; Guo, H. Efficient Visible to Near-Infrared Energy Transfer in Ce^{3+}-Yb^{3+} Co-Doped Y_2SiO_5 Phosphors. *Opt. Mater.* **2012**, *34*, 1034−1036.
(47) Wu, D.; Xiao, W.; Zhang, L.; Zhang, X.; Hao, Z.; Pan, G. H.; Luo, Y.; Zhang, J. Simultaneously Tuning the Emission Color and Improving Thermal Stability via Energy Transfer in Apatite-Type Phosphors. *J. Mater. Chem. C* **2017**, *5*, 11910−11919.
(48) Xiao, Y.; Hao, Z.; Zhang, L.; Zhang, X.; Pan, G. H.; Wu, H.; Wu, H.; Luo, Y.; Zhang, J. Efficient Green Phosphor of Ce^{3+} and Tb^{3+} Codoped $Ba_2Lu_5B_5O_{17}$ and a Model for Elucidating the High Thermal Stability of the Green Emission. *J. Mater. Chem. C* **2018**, *6*, 5984−5991.
(49) Feng, L.; Hao, Z.; Zhang, X.; Zhang, L.; Pan, G.; Luo, Y.; Zhang, L.; Zhao, H.; Zhang, J. Red Emission Generation through

DOI: 10.1021/acs.inorgchem.8b02304
Inorg. Chem. XXXX, XXX, XXX−XXX

Highly Efficient Energy Transfer from Ce^{3+} to Mn^{2+} in CaO for Warm White LEDs. *Dalton T.* **2016**, *45*, 1539−1545.
(50) Barbosagarcia, O.; Mcfarlane, R. A.; Birnbaum, M.; Diaztorres, L. A. Neodymium-to-Erbium Nonradiative Energy Transfer and Fast Initial Fluorescence Decay of the $^4F_{3/2}$ State of Neodymium in Garnet Crystals. *J. Opt. Soc. Am. B* **1997**, *14*, 2731−2734.
(51) Barandiaran, Z.; Meijerink, A.; Seijo, L. Configuration Coordinate Energy Level Diagrams of Intervalence and Metal-to-Metal Charge Transfer States of Dopant Pairs in Solids. *Phys. Chem. Chem. Phys.* **2015**, *17*, 19874−19884.
(52) Zhong, Y.; Ma, Z.; Zhu, S.; Yue, J.; Zhang, M.; Antaris, A. L.; Yuan, J.; Cui, R.; Wan, H.; Zhou, Y.; Wang, W.; Huang, N. F.; Luo, J.; Hu, Z.; Dai, H. Boosting the Down-Shifting Luminescence of Rare-Earth Nanocrystals for Biological Imaging beyond 1500 nm. *Nat. Commun.* **2017**, *8*, 737.
(53) Zhou, L.; Tanner, P. A.; Zhou, W.; Ai, Y.; Ning, L.; Wu, M. M.; Liang, H. Unique Spectral Overlap and Resonant Energy Transfer between Europium (II) and Ytterbium (III) Cations: No Quantum Cutting. *Angew. Chem.* **2017**, *129*, 10493−10497.
(54) Huang, X. Y.; Yu, D. C.; Zhang, Q. Y. Enhanced Near-Infrared Quantum Cutting in $GdBO_3$: Tb^{3+}, Yb^{3+} Phosphors by Ce^{3+} Codoping. *J. Appl. Phys.* **2009**, *106*, 113521.
(55) Guille, A.; Pereira, A.; Breton, G.; Bensalah-Ledoux, A.; Moine, B. Energy Transfer in $CaYAlO_4$: Ce^{3+}, Pr^{3+} for Sensitization of Quantum-Cutting with the Pr^{3+}-Yb^{3+} Couple. *J. Appl. Phys.* **2012**, *111*, No. 043104.
(56) Sun, T.; Chen, X.; Jin, L.; Li, H. W.; Chen, B.; Fan, B.; Moine, B.; Qiao, X.; Fan, X.; Tsang, S. W.; Yu, S. F.; Wang, F. Broadband Ce (III)-Sensitized Quantum Cutting in Core−Shell Nanoparticles: Mechanistic Investigation and Photovoltaic Application. *J. Phys. Chem. Lett.* **2017**, *8*, 5099−5104.

DOI: 10.1021/acs.inorgchem.8b02304
Inorg. Chem. XXXX, XXX, XXX−XXX